RESEARCH ARTICLE

RNA Futile Cycling in Model Persisters Derived from MazF Accumulation

Wendy W. K. Mok,[a] Junyoung O. Park,[a,b] Joshua D. Rabinowitz,[b,c] Mark P. Brynildsen[a]

Department of Chemical and Biological Engineering, Princeton University, Princeton, New Jersey, USA[a]; Lewis-Sigler Institute for Integrative Genomics, Princeton University, Princeton, New Jersey, USA[b]; Department of Chemistry, Princeton University, Princeton, New Jersey, USA[c]

ABSTRACT **Metabolism plays an important role in the persister phenotype, as evidenced by the number of strategies that perturb metabolism to sabotage this troublesome subpopulation. However, the absence of techniques to isolate high-purity populations of native persisters has precluded direct measurement of persister metabolism. To address this technical challenge, we studied *Escherichia coli* populations whose growth had been inhibited by the accumulation of the MazF toxin, which catalyzes RNA cleavage, as a model system for persistence. Using chromosomally integrated, orthogonally inducible promoters to express MazF and its antitoxin MazE, bacterial populations that were almost entirely tolerant to fluoroquinolone and β-lactam antibiotics were obtained upon MazF accumulation, and these were subjected to direct metabolic measurements. While MazF model persisters were nonreplicative, they maintained substantial oxygen and glucose consumption. Metabolomic analysis revealed accumulation of all four ribonucleotide monophosphates (NMPs). These results are consistent with a MazF-catalyzed RNA futile cycle, where the energy derived from catabolism is dissipated through continuous transcription and MazF-mediated RNA degradation. When transcription was inhibited, oxygen consumption and glucose uptake decreased, and nucleotide triphosphates (NTPs) and NTP/NMP ratios increased. Interestingly, the MazF-inhibited cells were sensitive to aminoglycosides, and this sensitivity was blocked by inhibition of transcription. Thus, in MazF model persisters, futile cycles of RNA synthesis and degradation result in both significant metabolic demands and aminoglycoside sensitivity.**

IMPORTANCE **Metabolism plays a critical role in controlling each stage of bacterial persistence (shutdown, stasis, and reawakening). In this work, we generated an *E. coli* strain in which the MazE antitoxin and MazF toxin were artificially and independently inducible, and we used this strain to generate model persisters and study their metabolism. We found that even though growth of the model persisters was inhibited, they remained highly metabolically active. We further uncovered a futile cycle driven by continued transcription and MazF-mediated transcript degradation that dissipated the energy derived from carbon catabolism. Interestingly, the existence of this futile cycle acted as an Achilles' heel for MazF model persisters, rendering them vulnerable to killing by aminoglycosides.**

Received 21 September 2015 **Accepted** 19 October 2015 **Published** 17 November 2015

Citation Mok WWK, Park JO, Rabinowitz JD, Brynildsen MP. 2015. RNA futile cycling in model persisters derived from MazF accumulation. mBio 6(6):e01588-15. doi:10.1128/mBio.01588-15.

Editor Gerard D. Wright, McMaster University

Address correspondence to Mark P. Brynildsen, mbrynild@princeton.edu.

Bacterial persisters were first described by J. W. Bigger over 70 years ago, and these phenotypic variants have since been documented for a wide range of microbial species treated with many different antibiotics (1, 2). Despite garnering less attention than antibiotic resistance, persistence is of considerable clinical concern, as persisters contribute to antibiotic failure and relapse of infections and serve as a reservoir from which resistant strains could emerge (1, 3–6). Unlike resistant bacteria, persisters arise in an isogenic population and generally do not grow in the presence of antibiotics (7), although exceptions have been noted for prodrugs that require activation (8). Rather, they are rare phenotypic variants that can subsist during treatment with high antibiotic concentrations. Once the course of treatment terminates, persisters can exit this transient state, resume growth, and give rise to progeny that exhibit the same antibiotic sensitivity as the parent (6, 7).

Persisters were traditionally thought to arise from slowly growing or nongrowing bacteria with reduced metabolic activity, where antibiotic targets are inactive and resilient to antibiotic corruption (1). In recent studies, our group and others have shown that a number of metabolic pathways remain functional during persistence, allowing persisters to generate proton motive force upon consumption of different metabolites (9–12). Metabolism is an important regulator in bacterial persisters (reviewed in references 13 and 14), as demonstrated by the number of metabolic genes (15–18) and metabolic stresses (19–21) involved in their formation. In particular, persistence can be framed as a metabolic program, where coordinated metabolic shutdown, maintenance, and reactivation drive the entry into, subsistence of, and exit from this transient nonreplicative state (14). Given the central role of metabolism in bacterial persistence, it is not surprising that a number of antipersister strategies that have been developed exert

their effects by targeting metabolism (9–11, 22, 23). For instance, one method involves stimulation of persisters with specific carbon sources that promote proton motive force generation, which leads to aminoglycoside uptake and persister killing (9, 10, 12). In another approach, Kim and colleagues identified a compound through a chemical screen that could stimulate the reversions of persisters to a replicating state and promote fluoroquinolone killing (23). These strategies further emphasize the potential and necessity of understanding persister metabolism in the development of novel methods for their effective elimination.

One major hurdle impeding research in persister metabolism is the lack of a robust isolation method that can segregate persisters from other cell types, specifically, viable but nonculturable cells (VBNCs), and yield highly pure samples of native persisters for direct metabolic measurements (9, 24–26). As persistence is a rare and transient phenotype, which is lost upon growth resumption, culturing of survivors does not yield persister populations (7). A number of attempts to isolate native persisters have been described, including methods based on β-lactam (27) or chemoenzymatic lysis of nonpersisters (28) and the use of fluorescent growth reporters to segregate fast-growing cells from their dormant kin (29). Although some of these methods succeeded in providing persister-enriched populations, those populations were not of sufficient purity for measurements to be solely reflective of persister physiology (9, 25). To circumvent these isolation challenges, researchers have used methods to produce "synthetic" or "model" persisters, such as overexpressing toxins, which have been implicated as terminal effectors of the persister phenotype (19, 30–32), or treating bacterial cultures with chemical inhibitors (33) to increase the abundance of persister-like cells in a population. These persister analogs can then be subjected to transcriptome, proteome, or metabolome analyses, to study antibiotic-tolerant states that mimic persistence.

Among the genes that are linked to persistence is a subset known to encode toxin-antitoxin (TA) modules, which are distributed across diverse microbial genomes (reviewed in references 34 and 35). These ubiquitous two-component systems consist of a stable protein toxin and a labile antitoxin, which may be an RNA or a protein, with the exception of ppGpp-SpoT, which comprises a new type of module where a metabolic network exhibits TA properties (19). Antitoxins can either inhibit the production of their cognate toxins or antagonize their activities. The TA systems identified to date are classified based on the nature of antitoxins and mechanism by which they inhibit their cognate toxins (36). Each toxin can also target different cellular components, including RNAs, enzymes, and the inner membrane, ultimately leading to growth inhibition (35). Although the biological roles of most TA modules remain unclear, many are emerging as key stress regulatory elements and terminal effectors of persistence (reviewed in references 37 and 38). MazEF is a type II TA system in which the proteinaceous MazF toxin is sequestered by the MazE protein antitoxin in the off state (39). When MazF is liberated from MazE sequestration, it acts as an endoribonuclease, cleaving target RNAs at ACA sites (40) and inhibiting protein synthesis (41). The activity of MazF has been implicated in two opposing cell fates: programmed cell death (39, 42) and reversible growth stasis and enhanced persistence (43, 44).

In an earlier study, Bokinsky and colleagues overexpressed HipA, another type II toxin, to produce β-lactam tolerant model persisters, which could be used for metabolite quantification, as well as glucose uptake and oxygen consumption measurements (30). Given that MazF production has also been linked to persistence (31, 44), we sought to generate model persisters with MazF accumulation for metabolic measurements. We synthesized an *Escherichia coli* strain in which the expression of *mazE* and *mazF* could be orthogonally induced from the chromosome. We demonstrated that when MazF was produced in amounts exceeding that of MazE, reversible stasis was achieved and treatment of the population with β-lactam and fluoroquinolone antibiotics did not result in significant killing. When we quantified the metabolism of the MazF persisters, we found that cells maintained impressive oxygen consumption and glucose uptake during growth stasis, which was suggestive of an increase in futile cycling. When metabolomic analyses of MazF persisters were performed, we observed high NMP levels, which provided evidence for RNA futile cycling in these model persisters. In consideration of the metabolic data and the mode of action of MazF, we hypothesized that a macromolecular futile cycle was formed where energy was consumed by transcription only for the transcripts to be degraded by MazF. In support of this hypothesis, we observed reductions in oxygen consumption, glucose uptake, and NMP abundance in conjunction with increases in NTP abundance with transcriptional inhibition, but not translational inhibition. We also investigated the possible consequences of maintaining this RNA futile cycle on persister antibiotic tolerance, and discovered that continued transcription sustained sufficient translational activity to render MazF-inhibited cells susceptible to killing by aminoglycosides (AGs).

RESULTS

MazF accumulation results in reversible growth stasis and enhanced antibiotic tolerance. Motivated by the therapeutic potential of targeting persister metabolism and the isolation challenges associated with obtaining native persister cells, we sought to generate a population of model persisters with MazF accumulation and examine the metabolic program of this type of persister. To produce *E. coli* strains with an orthogonally controlled *mazE-mazF* expression system and to prevent phenotypic heterogeneity attributed to plasmid copy number variation, we replaced endogenous *mazEF* with inducible copies integrated at two distinct loci of the chromosome (see Fig. S1A to D in the supplemental material). In this design, *mazE* is controlled by P_{BAD}, and its expression is inducible with arabinose (Ara), while *mazF* is regulated by P_{LtetO1} (45) and is inducible with anhydrotetracycline (aTc). To mimic changes in gene expression that naturally lead to the accumulation of MazF in *E. coli*, we induced *mazE* expression with Ara at the time of inoculation, and aTc was added after approximately one doubling to induce *mazF*. This allowed the toxin to be sequestered by the antitoxin as it was expressed, thereby preventing growth inhibition and allowing cells to enter the exponential phase of growth. Once cells were in exponential phase, cells were diluted in medium with only aTc, allowing MazF to be accumulated in excess of MazE. As a control, an identical aliquot of cells was diluted in medium with aTc and Ara to allow TA coexpression.

We observed that the accumulation of MazF in excess of MazE resulted in growth inhibition after 2 h, whereas cells expressing both MazE and MazF continued to grow (Fig. 1A and B; note that the increase in optical density at 600 nm [OD_{600}] but lack of increase in CFU for MazF-accumulating cultures most likely reflects

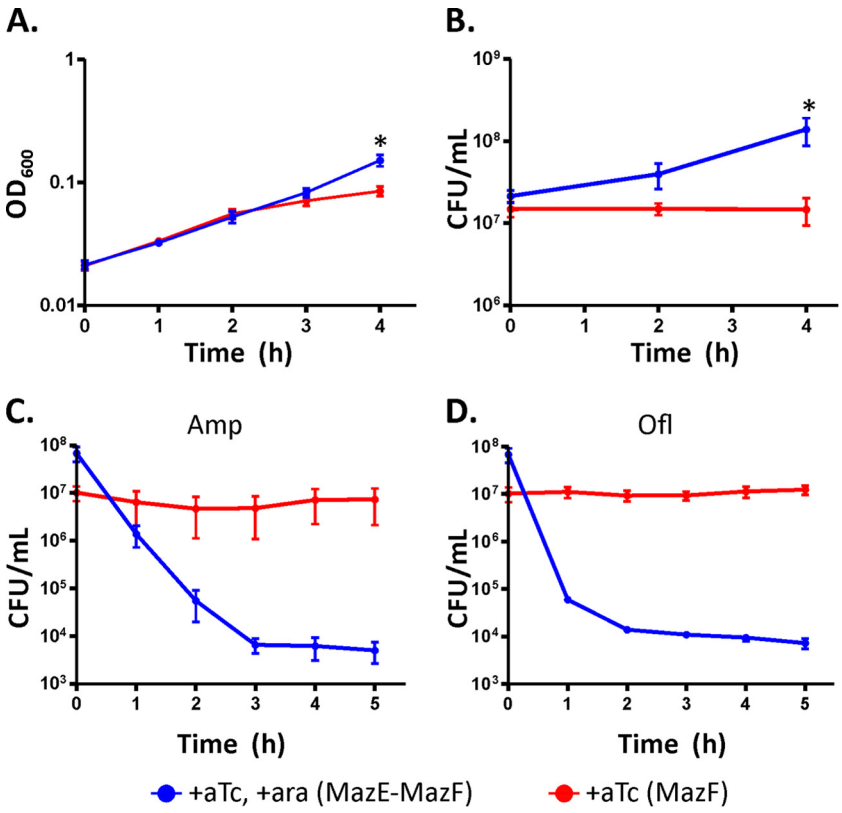

FIG 1 Growth, culturability, and persistence of *E. coli* MO::*mazE-mazF*. *E. coli* MO::*mazE-mazF* was cultured in growth medium supplemented with aTc and Ara for MazE-MazF coexpression (blue lines) or with only aTc to facilitate MazF accumulation (red lines). Accumulation of MazF in excess of MazE resulted in bacteriostasis, as determined by OD_{600} measurements (A) and CFU counts (B). OD_{600} and CFU counts between these cells and the MazE-MazF coexpression control were significantly different at 4 h (*, $P < 0.05$). When a majority of cells in the MazF-accumulating populations were in a reversible growth-arrested state (4 h after MazF accumulation), significant killing from treatment with Amp (C) and Ofl (D) was not observed, demonstrating that MazF-induced growth arrest produced model persisters. In comparison, the MazE-MazF coexpression control was susceptible to both antibiotics and exhibited biphasic killing.

the reduced temporal resolution and accuracy of CFU measurements, which is supported by flow cytometry-based cell counting, where numbers of cells per milliliter and CFU per milliliter never differed significantly [see Fig. S2A in the supplemental material]). Similarly, dilution of *E. coli* MO::*mazE*, which lacks P_{LtetO1}-*mazF*, in medium with only aTc did not result in growth inhibition, demonstrating that stasis was dependent on MazF accumulation (see Fig. S2B in the supplemental material). These results demonstrated that toxin overexpression in our system led to reversible growth stasis without reducing culturability, which is consistent with some previous studies of MazF (31, 43, 44).

We then examined the impact of MazF accumulation on persistence toward antibiotics from two distinct classes: ampicillin (Amp; a cell wall biosynthesis inhibitor) and ofloxacin (Ofl; a DNA gyrase inhibitor). To ensure that the cells had achieved growth stasis at the time of the assay, persister measurements of the MazF-accumulating samples were taken 4 h following the dilution in aTc-supplemented medium. MazE-MazF-expressing samples were taken 3 h following dilution, so that their densities were comparable to those of the MazF samples. With the MazE-MazF samples, we observed biphasic killing following treatment with both Amp and Ofl, which resulted in reductions in numbers of CFU per milliliter of approximately 4 orders of magnitude (Fig. 1C and D). Importantly, MazF samples exhibited tolerance to Amp and Ofl that approached 100%, with CFU counts before and after 5 h of individual antibiotic treatments being approximately equivalent and not statistically significantly different. These observations confirmed that the vast majority, if not all, of MazF-accumulating cells were Amp and Ofl persisters.

MazF persisters continue to consume oxygen and glucose during growth stasis. Native persisters predominantly arise from dormant, nongrowing subpopulations, yet they retain metabolic activity, as demonstrated by the consumption of an array of carbon sources to drive respiration and produce proton motive force (9, 10). Here, we sought to elucidate the metabolic capacity of cells undergoing MazF accumulation by quantifying their oxygen and glucose consumption as they entered and remained in toxin-induced bacteriostasis. To measure the dissolved oxygen in cell cultures, cells were cultured in a bioreactor, in which MazE-MazF samples were able to grow and MazF-accumulating samples achieved stasis within 2.5 to 3 h of the initiation of MazF accumulation, which was similar to results obtained from flasks (Fig. 2A). We observed that MazF and MazE-MazF samples initially consumed oxygen at comparable rates (Fig. 2B). With the onset of toxin-induced growth inhibition, total oxygen consumption in the MazF-accumulating culture decreased, and a similar trend was observed for glucose consumption (Fig. 2C). However, total oxygen consumed relative to glucose consumed in MazF-arrested cells was ~50% higher than that in the coexpression control (Fig. 2D). Further, oxygen consumption relative to biomass pro-

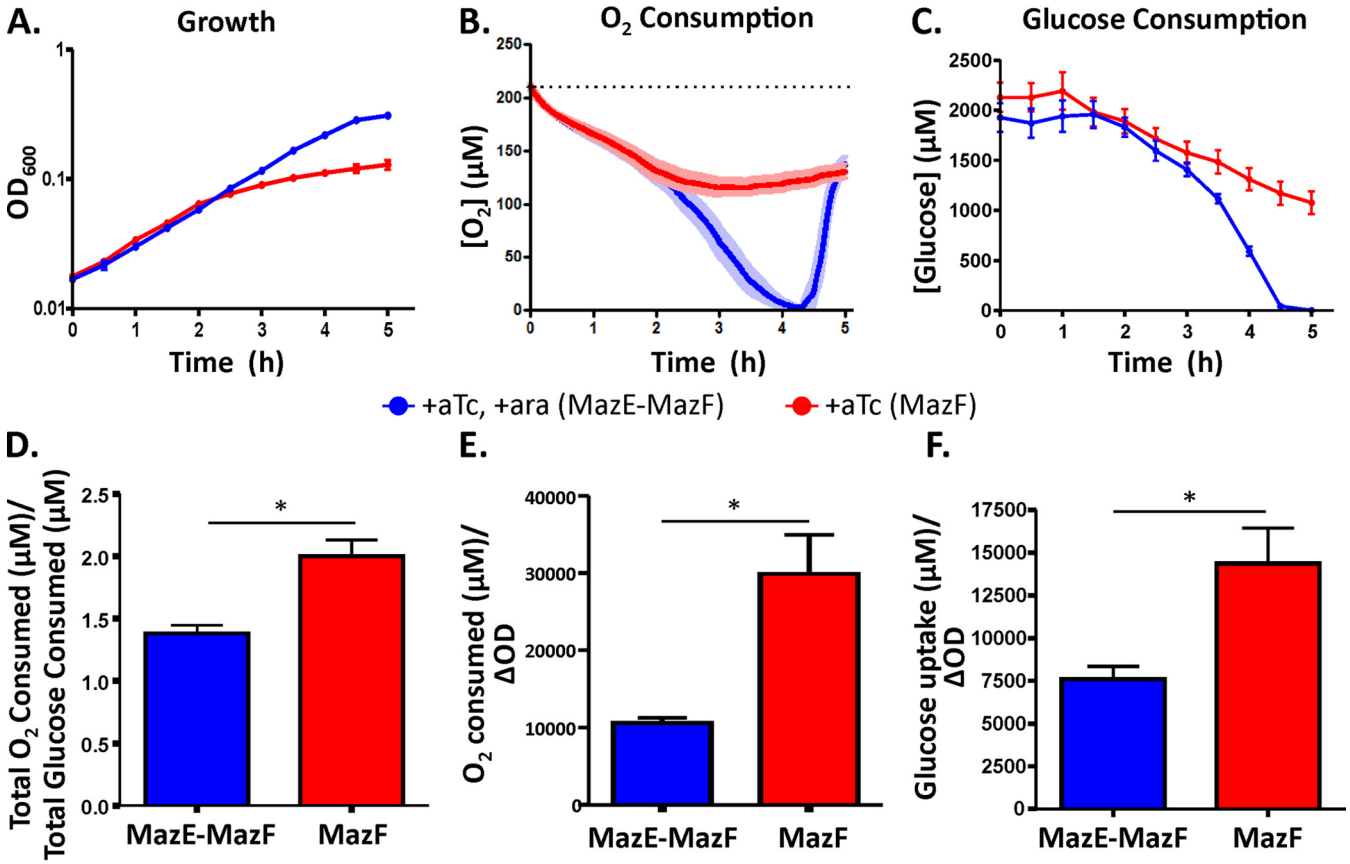

FIG 2 Quantification of oxygen and glucose consumption in MazF model persisters. *E. coli* MO::*mazE-mazF* was grown to exponential phase before being washed and diluted in Gutnick with 2 mM glucose supplemented with aTc for MazF accumulation (red lines) or aTc with Ara for MazE-MazF coexpression (blue lines) at 0 h. (A) Growth of *E. coli* accumulating MazF or both MazE and MazF in the bioreactor where oxygen measurements were performed. (B) Oxygen consumption of cells accumulating MazF or expressing MazE-MazF measured over 5 h following inoculation in the bioreactor. The equilibrium oxygen concentration of the medium was 210 μM (dashed line). Cells undergoing MazF-mediated growth inhibition continued to consume oxygen, as illustrated by the concentration of dissolved oxygen in the growth medium remaining below 210 μM. (C) Glucose consumption of cells accumulating MazF or MazE-MazF. In the MazF samples, glucose consumption continued during growth inhibition. In the MazE-MazF sample, glucose exhaustion occurred around 4.5 h, and the cessation of glucose consumption coincided with an increase in dissolved oxygen in the growth medium. (D) Oxygen consumed per glucose consumed was calculated using data points from 2.5 to 5 h. Cells accumulating MazF consumed ~50% more oxygen per glucose compared with the MazE-MazF coexpression control. (E) Oxygen consumed relative to biomass produced was calculated using data points from 2.5 to 5 h, and it was 2.8-fold higher in MazF-inhibited cells than in cells expressing MazE-MazF. (F) Glucose consumed relative to biomass produced (calculated using data points from 2.5 to 5 h) was 1.9-fold higher than that of the coexpression control. *, $P \leq 0.05$.

duction (29,892 ± 5,051 μM/OD unit produced) was 2.8-fold higher than the normally growing MazE-MazF control (10,592 ± 688 μM/OD unit produced) (Fig. 2E), and glucose consumption per biomass produced during MazF-induced growth inhibition (14,368 ± 2,070 μM/OD unit produced) was 1.9-fold higher than that of the MazE-MazF control (7,613 ± 739 μM/OD produced) (Fig. 2F). Results from these experiments demonstrate that during MazF-induced shutdown, cells continued to consume oxygen and glucose without producing much biomass, and a higher proportion of glucose consumed was catabolized to drive respiration, which is the main consumer of oxygen under the conditions used here (46). This inefficient use of energy is a hallmark of cells undergoing increased futile cycling (47, 48).

MazF accumulation depresses cellular energy levels. To further investigate the metabolic changes in cells during toxin-induced shutdown, we analyzed the metabolomes of MazF-accumulating cells by liquid chromatography-mass spectrometry (LC-MS) (see Fig. S3 in the supplemental material) (49). We compared the abundance of metabolites extracted from MazF-accumulating cells with that of metabolites extracted from cells coexpressing MazE-MazF to identify the metabolites whose abundance significantly changed as a result of toxin-induced stasis. To assess whether the addition of aTc or Ara impacted the metabolome, we additionally extracted metabolites from *E. coli* MO::*mazE* treated with aTc, which resulted in no protein induction, or with aTc and Ara, which induced MazE. To capture MazF-accumulating cells during their transition from a growing state to a nongrowing state, samples were collected 2, 3, and 4 h following dilution into medium supplemented with the appropriate inducers.

As cells entered MazF-induced growth stasis, we observed the most striking changes in the abundance of nucleotides (see Fig. S3 in the supplemental material). For each strain, we calculated the ratios of the abundances of ribonucleotides from cells treated with aTc to those from cells treated with both aTc and Ara (i.e., uninduced/MazE for *E. coli* MO::*mazE* and MazF/MazE-MazF for

E. coli MO::*mazE-mazF*). We observed that in MazF-accumulating cells, the abundance of all 4 nucleotide monophosphates (NMPs) increased 5- to 9-fold over time (Fig. 3). Furthermore, we detected increases in nucleotide diphosphates (NDPs). Although statistically significant increases in some NTPs were observed, they were all modest compared to the increases in the NMPs. We note that large changes in NMP or NDP levels do not have to be accompanied by reciprocal changes in NTP levels, because the concentrations of NTPs in *E. coli* are around 10-fold higher than the concentrations of NMPs and NDPs (50). In MazF-accumulating cells, the relative increases in NMPs and NDPs were higher than those of their NTP counterparts, which translates to a lower energy charge, as classically defined by the expression ([NTP] + 0.5[NDP])/([NTP] + [NDP] + [NMP]) (51). The elevation in NMPs and NDPs complemented the oxygen and glucose consumption data (Fig. 2) in supporting the hypothesis of increased futile cycling in MazF-inhibited cells (47, 48). As MazF is an endoribonuclease, which cleaves target transcripts at ACA sites (40), we hypothesized that the abundance of NMPs, which was coincident with MazF-mediated growth arrest, was a result of continued transcription followed by RNA degradation, where NMPs are the direct molecular products. As depicted in Fig. 4, this would result in a macromolecular (transcription/transcript degradation) futile cycle, where energy is expended without producing a gain in biomass.

Transcriptional inhibition reduces oxygen and glucose consumption. To test the above hypothesis and determine whether transcription is a major energy sink in MazF-inhibited cells, we inhibited transcription with Rif and measured oxygen and glucose consumption thereafter. Cells were also treated with spectinomycin (Spec) and KCN to compare the effects of translational inhibition and electron transport chain inhibition with those of transcriptional inhibition. When MazF-accumulating cells were treated with Rif, oxygen consumption decreased rapidly, reaching a new steady state within 30 min (Fig. 5A). This pattern of rapid inhibition of oxygen consumption qualitatively mirrored that of cells treated with KCN, which inhibits cytochrome oxidase activity (Fig. 5B). As MazF already reduces protein synthesis through cleavage of both mRNA and rRNA (40, 52), inhibiting translation with Spec did not and was not expected to reduce oxygen consumption (Fig. 5C). Rif also transiently decreased glucose consumption (Fig. 5D). Combined, these results suggested that RNA polymerase activity is a driving force for energy consumption in MazF-inhibited cells, which supported the hypothesis that MazF accumulation initiated an RNA futile cycle.

Transcriptional inhibition impedes MazF-dependent depression of cellular energy levels. We investigated the effect of Rif and Spec treatment on the nucleotide pools in MazF-accumulating cells (Fig. 6). In the case of the purine nucleotides, we observed significant decreases in AMP, ADP, GMP, and GDP levels in Rif-treated, MazF-accumulating cells compared with the untreated control, whereas the abundances of ATP and GTP increased 2.5- and 6-fold, respectively. In contrast, treatment with Spec did not significantly alter the abundances of any purine nucleotide in comparison to the untreated control. For uridine nucleotides, a largely similar pattern was observed, except that UDP levels in Rif-treated samples were not significantly different from those of the untreated control. However, cytosine nucleotides had a distinct pattern, where Rif treatment significantly increased the abundance of CMP, CDP, and CTP compared to untreated controls, whereas Spec treatment changed them very little. Although the origin of this metabolic perturbation of cytosine nucleotides was not determined here, we did find that significant accumulation of cytosine nucleotides also occurred in Rif-treated *E. coli* MO::*mazE* induced with aTc, whereas the other Rif-dependent nucleotide perturbations in MazF-accumulating cells were not observed (see Fig. S4 in the supplemental material). These data suggested that the changes in cytosine nucleotide levels originated from a Rif-dependent phenomenon that was independent of MazF, whereas the changes in purine and uridine nucleotide levels reflected an interaction between MazF and transcriptional inhibition. Overall, NTP/NMP ratios were greatly increased by Rif for all nucleotides, which provides further support for the idea that MazF accumulation depressed energy levels through a futile cycle driven by RNA polymerase (RNAP) and the toxin's endoribonuclease activity.

Effect of futile cycle inhibition on antibiotic tolerance. To further study the impacts of the transcription/RNA degradation futile cycle, we examined the effect of inhibiting this cycle on tolerance of different classes of antibiotics (Fig. 7). When Rif-treated cells were plated, we observed ~10-fold fewer CFU than their untreated counterparts at time zero, and CFU counts increased throughout the course of the 5-h assay. These changes in CFU were observed even in the absence of subsequent antibiotic treatment (Fig. 7A), suggesting that they were Rif dependent. These changes in CFU counts could be due to a fraction of the population being killed immediately from Rif treatment followed by replication of the surviving population over the next 5 h, or alternatively, the increase in CFU could be attributed to cells regaining culturability over time. To determine which of the two mechanisms was behind the changes in CFU counts observed in Rif-treated cells, we used the IPTG-inducible copy of the mCherry gene integrated in place of *lacZYA* in *E. coli* MO::*mazE* and *E. coli* MO::*mazE-mazF* as a cell division reporter (53). IPTG was added to induce expression of the mCherry gene at the same time as aTc addition, when cells were being cultured from lag phase to early exponential phase. When cells reached an OD_{600} of 0.1, they were pelleted and washed before being diluted in fresh medium, thereby removing the IPTG. We then monitored changes in red fluorescence in these cells before and after Rif treatment using flow cytometry. If the cells were dividing, mCherry would be distributed among the daughter cells, and a reduction in the mean fluorescence of the population would be observed over time (53). If the cells were regaining culturability after Rif treatment, dilution of red fluorescence would not be observed.

We measured the fluorescence of the population at 3 h, which was just before Rif treatment. Samples were also measured at 4 h and 9 h, which correspond to 0 h and 5 h of persister assays. In cells accumulating MazF, we observed that the mean fluorescence of the population decreased to ~40% in 4 h as cells divided before reaching a plateau as growth was inhibited by MazF. The mean fluorescence of the population then remained at ~30% (see Fig. S5A in the supplemental material). In *E. coli* accumulating MazF treated with Rif, the decrease in red fluorescence also reached a plateau by 4 h and remained at ~30% by 9 h (see Fig. S5B in the supplemental material). As a control, we monitored the growth and fluorescence of *E. coli* MO::*mazE*, and we observed that this population, which grew exponentially, displayed a sigmoidal decline in mean population fluorescence and approached 0% by 6 h (see Fig. S5C in the supplemental material). When this

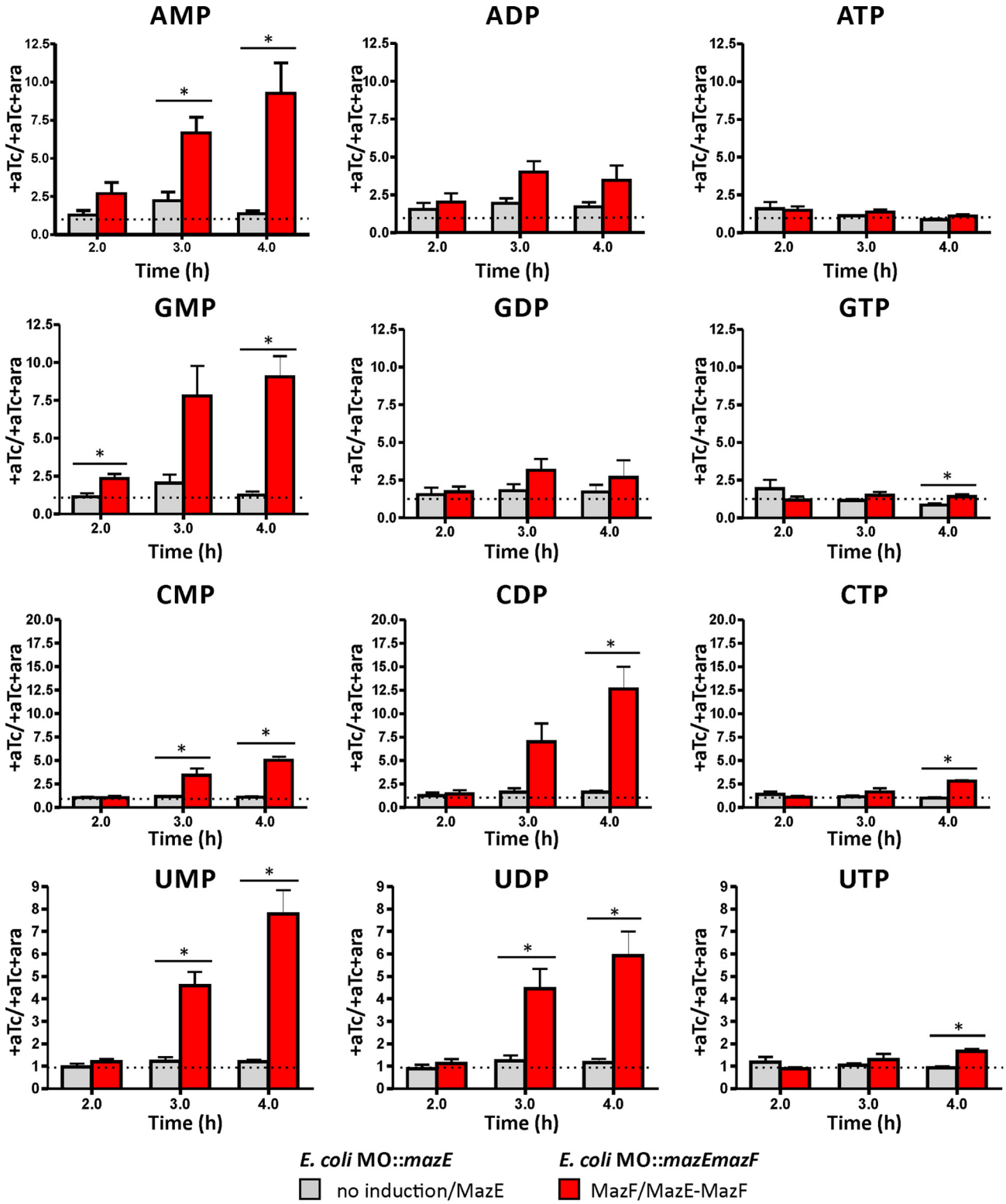

FIG 3 Quantification of ribonucleotide pools in MazF model persisters during growth stasis. *E. coli* MO::*mazE* and *E. coli* MO::*mazE-mazF* were grown to exponential phase before being washed and diluted in Gutnick-glucose medium supplemented with aTc or aTc and Ara, which represents 0 h. Samples were collected and extracted 2, 3, and 4 h postdilution. Ratios of ribonucleotides in *E. coli* MO::*mazE* and *E. coli* MO::*mazE-mazF* were calculated by dividing the OD_{600}-normalized abundances in aTc-induced cells by the OD_{600}-normalized abundances in aTc and Ara-induced cells collected from the same experimental replicate. Averages and standard errors of the means (SEM) of ratios calculated from four experiments are shown. Ratios derived from *E. coli* MO::*mazE-mazF* were compared with ratios derived from *E. coli* MO::*mazE* (*, $P \leq 0.05$). Overall, MazF accumulation resulted in statistically significant increases in all four ribonucleotide monophosphates. Greater relative increases in the abundances of NMPs and NDPs compared with their NTP counterparts are suggestive of low energy levels in MazF-accumulating cells.

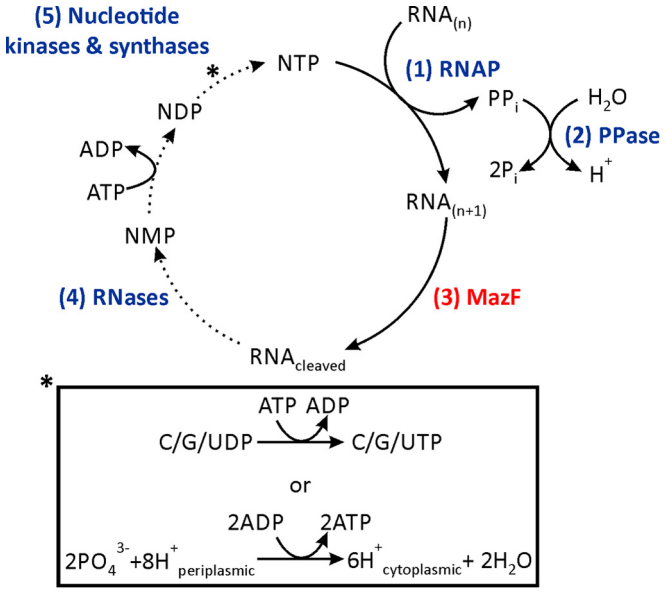

FIG 4 MazF-induced transcription/transcript degradation macromolecular futile cycle. (Step 1) Transcription mediated by RNAP is hypothesized to continue in MazF model persisters. (Step 2) Hydrolysis of pyrophosphates by inorganic pyrophosphatase (PPase) provides thermodynamic pull for RNA synthesis. (Step 3) RNAs are cleaved by MazF. (Step 4) Various RNases further degrade cleaved RNA ($RNA_{cleaved}$), leading to NMP accumulation. (Step 5) Nucleotide kinases and synthases catalyze the phosphorylation of NMPs to produce NTPs, which is a process that consumes energy.

population was treated with Rif 3 h postdilution, the decrease in fluorescence slowed, reached a plateau by 4 h, and remained at ~25% (see Fig. S5D in the supplemental material). These observations suggest that if the Rif-treated samples were to grow 10-fold in 5 h, it should present as an almost complete loss of fluorescence, similar to the decline observed with the MazE control between 3 and 7 h. The lack of decrease in mean population fluorescence demonstrates that the increase in CFU observed in Rif-treated samples was not due to growth in the presence of antibiotics but was rather a result of cells regaining culturability over time.

While transcription inhibition with Rif affected culturability soon after treatment, it did not alter the tolerance of MazF-accumulating cells to Amp (Fig. 7B) and Ofl (Fig. 7C), as Rif-treated and untreated samples produced comparable CFU counts after 5 h of antibiotic exposure. While MazF acts as an endoribonuclease, cells accumulating MazF have been shown to retain some translational activity, being able to translate synthetic mRNAs devoid of the ACA recognition sequence as well as a subset of native transcripts (41, 54). Although rRNAs are protected from extensive degradation by structures and ribosomal proteins, Vesper and colleagues found that the anti-Shine-Dalgarno sequence of the 16S rRNA was susceptible to MazF cleavage, thereby producing "stress ribosomes" that favor the translation of mRNAs lacking the leader sequence upstream of their start codons (52). Consistent with these findings, we observed that cells accumulating MazF could transcribe and translate the IPTG-inducible mCherry gene during stasis, producing fluorescent cells (see Fig. S6A in the supplemental material). This evidence of translational activity in MazF-arrested cells led us to investigate their sensitivity to kanamycin (Kan) and streptomycin (Strep), bactericidal members of the AG class of antibiotics, which target the aminoacyl-tRNA site and decoding center of the ribosome, respectively, and cause mistranslation (55–57). Unlike Amp and Ofl, *E. coli* accumulating MazF was as sensitive to Kan (Fig. 7D) and Strep (Fig. 7E) as *E. coli* MO::*mazE*, with numbers of CFU per milliliter decreasing by 4 to 5 orders of magnitude. When transcription was inhibited with Rif, which inhibited protein synthesis at an upstream step, protein synthesis was significantly reduced (see Fig. S6A in the supplemental material) and AG-enabled killing was no longer observed (Fig. 7D and E). To determine whether a perturbation of proton motive force contributed to AG tolerance upon Rif treatment, we used $DiBAC_4(3)$ to quantify membrane potential ($\Delta\psi$) (58). We note that at neutral pH, the dominant component of proton motive force, which is the main driving force for AG uptake, is $\Delta\psi$ (59, 60). Consistent with previous reports, we observed that $\Delta\psi$ was not diminished with Rif treatment (see Fig. S6B in the supplemental material) (61). Inhibiting RNAP activity with Rif in the *E. coli* MO::*mazE* control also conferred tolerance to Kan and Strep along with Ofl and Amp (see Fig. S7 in the supplemental material), which is consistent with a previous report (33). Thus, in MazF-inhibited cells, the residual translational activity that occurs as a result of operation of the RNA futile cycle (continued transcription in the face of MazF-mediated RNA degradation) (Fig. 4) is sufficient to support killing by aminoglycosides, and inhibition of the futile cycle at RNAP serves to expand the antibiotic tolerance profile of this type of persister.

DISCUSSION

Understanding persister metabolism is anticipated to produce novel targets for persister elimination (10, 14, 23), yet the absence of an effective method to isolate pure native persisters has prevented direct metabolic measurements and hindered progress in this area of research (9). With toxins of TA modules being increasingly identified as terminal effectors of the persister phenotype (34, 35), efforts have been made to achieve growth inhibition and antibiotic tolerance in bacteria with toxin overexpression (19, 31, 38, 62), which has allowed the metabolism of these model persisters to be assessed (30). The formation of native persisters has been proposed to involve multiple TA modules; thus, the activation of different TA modules has been postulated to contribute to the heterogeneity in persister populations (63). In this study, we sought to interrogate the metabolic program of persisters, and in the absence of methods to isolate native persisters to high purity, we relied upon MazF accumulation to produce a model system representative of one type of persister and analyzed its metabolic state. Consistent with several published reports, MazF accumulation in *E. coli* MO::*mazE-mazF*, where *mazE* and *mazF* were placed under the orthogonal control of two inducible promoters, resulted in reversible growth stasis without significant killing or loss of culturability (31, 43, 44). Furthermore, we observed enhanced persistence in the presence of fluoroquinolone and β-lactam antibiotics, as the resulting population could not be killed by Ofl or Amp (31, 44).

When extracellular metabolite consumption of MazF-inhibited cells was measured, we found that they, like cells inhibited by the HipA toxin examined previously (30), maintained active oxygen consumption and glucose uptake despite a significant reduction in biomass production. In fact, the oxygen and glucose consumption per biomass and amount of glucose consumed to drive respiratory activity all increased in cells undergoing MazF-

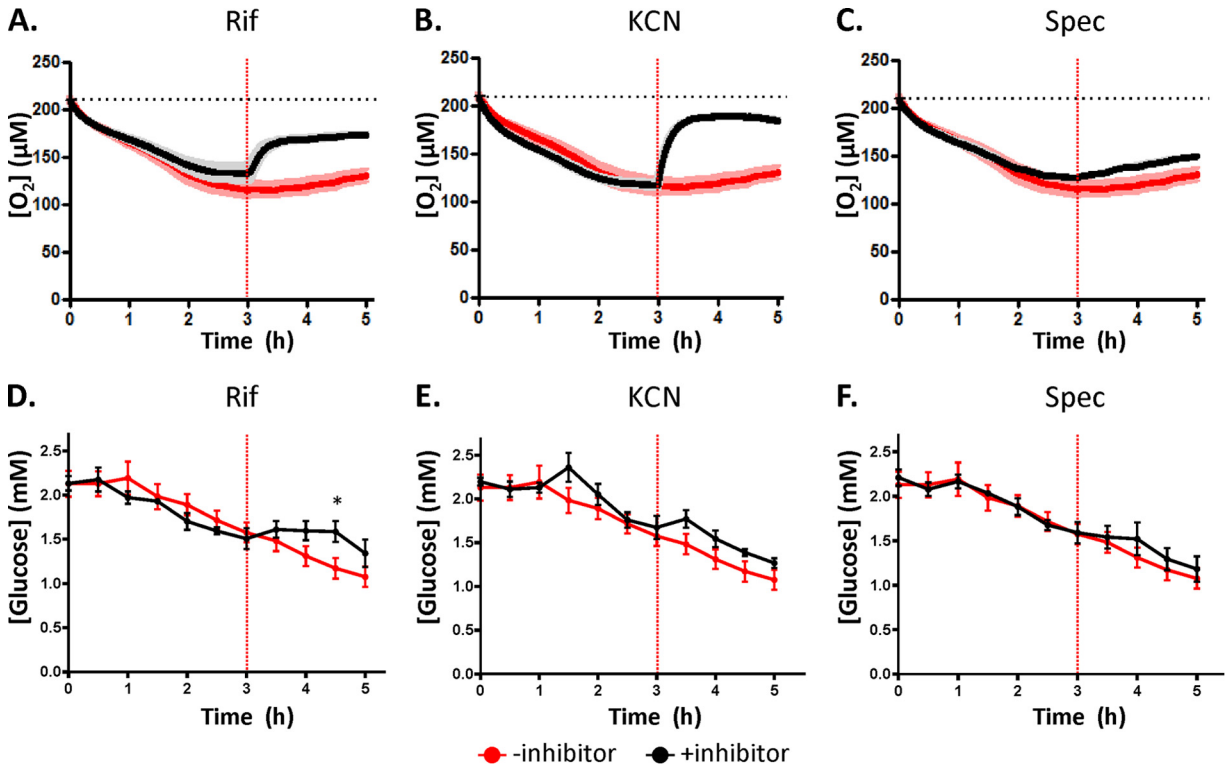

FIG 5 Effect of transcription and translation inhibitors on oxygen and glucose consumption in *E. coli* accumulating MazF. *E. coli* MO::*mazE-mazF* was grown to exponential phase and then pelleted, washed, and diluted in Gutnick medium with 2 mM glucose and aTc to induce MazF accumulation at 0 h. Dissolved oxygen and glucose consumption in the culture were measured in a bioreactor over 5 h. At 3 h postinoculation (red dashed line), inhibitors (100 μg/ml Rif, 100 μg/ml Spec, or 5 mM KCN) were added to each culture. Top panels compare oxygen consumption and bottom panels compare glucose consumption of untreated samples with those treated with Rif (A and D), KCN (B and E), or Spec (C and F). Inhibition of transcription in MazF-accumulating cells resulted in rapid decrease in oxygen consumption, which was similar to results with cells treated with the respiratory inhibitor KCN. Glucose consumption modestly and transiently decreased only in the Rif-treated sample, whereas cells treated with Spec or KCN exhibited glucose uptake similar to that in the untreated sample. *, $P \leq 0.05$.

induced growth inhibition compared with the MazE-MazF coexpression control, which was suggestive of futile use of resources (47, 48). When we analyzed the metabolomes of MazF-accumulating cells, we observed increased relative abundances of NMPs and NDPs compared with NTPs, which suggested that the energy level in these cells was reduced and provided additional evidence for enhanced futile cycling. The endoribonuclease activity of MazF led us to postulate that RNAP and MazF oppose each other's functions and establish an RNA (transcription/transcript degradation) futile cycle (Fig. 4). When we inhibited RNAP activity with Rif, we observed reductions in glucose and oxygen consumption, decreases in the abundance of most NMPs, and increases in the abundances of NTPs, which provided further support for the proposed futile cycle. We postulate that this futile cycle may function to continue synthesis of ribosomal RNAs, MazE, and other proteins (41), which could enable cells to overcome the inhibitory effects of MazF and resume growth rapidly.

Interestingly, the RNA futile cycle gives MazF model persisters an Achilles' heel. This cycle sustains aerobic respiration, which maintains an electrical potential ($\Delta\psi$) across the inner membrane, enabling AG uptake (see Fig. S6B in the supplemental material). Despite the function of MazF as an endoribonuclease, these cells retain residual protein synthesis, which renders this quasidormant population susceptible to killing by AG. Sensitivity to AGs in cells that are tolerant to quinolones and β-lactams has been well documented in native persisters (9, 10, 20, 24, 44, 64), and this points to a physiological parallel between the MazF model persisters used here and their native counterparts. Taken together with evidence that endoribonuclease toxins cross-activate (65) and are also integral to persister formation mediated by HipA (38), this macromolecular futile cycle, though found in MazF model persisters, may be a hallmark of cells undergoing growth arrest mediated by endoribonuclease toxins. As RNAs are cleaved, the toxin-arrested cells may attempt to counteract this catastrophic effect by replenishing RNAs, which produces a significant energy draw on the system. Metabolic analysis of model persisters generated with the accumulation of other type II endoribonuclease toxins are needed to determine whether this futile cycle is a common phenomenon.

In this study, we used MazF model persisters to investigate metabolic processes that remain active during shutdown and entry into a growth-inhibited, antibiotic-tolerant state. Metabolism in other stages of the persister metabolic program, such as the metabolic activities of MazF model persisters during long-term maintenance in the presence of antibiotics and the sequence of changes that drive reactivation and reawakening, remains to be investigated. Here, we showed that inhibiting the RNA futile cycle expanded the antibiotic tolerance profile of MazF model persisters. This further emphasizes that having a comprehensive view of the metabolic program of MazF model persisters, along with knowledge of the metabolic programs in model persisters formed

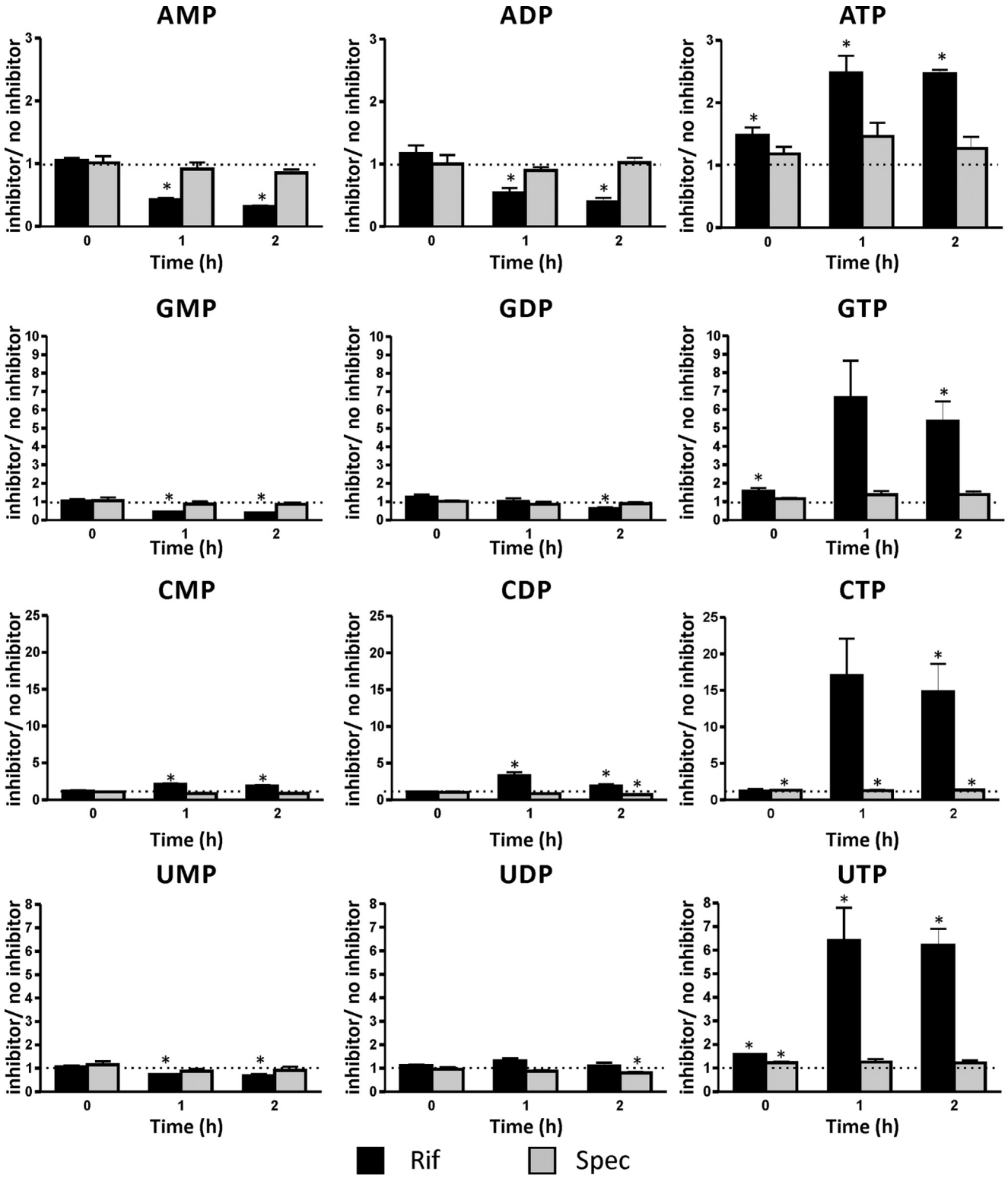

FIG 6 Effects of transcription and translation inhibitors on the ribonucleotide pools of MazF persisters. Three hours after *E. coli* MO::*mazE-mazF* was diluted and cultured in Gutnick-glucose with aTc to induce MazF accumulation (designated time zero), the samples were treated with no inhibitor, Rif, or Spec. Samples were then collected hourly for 2 h for LC-MS analysis. Ratios of ribonucleotides in inhibitor-treated samples to those in untreated samples were calculated by dividing the OD_{600}-normalized abundances in treated samples by the normalized abundances in untreated samples collected from the same experimental replicate. Averages and SEM of ratios calculated from four experiments are shown. A ratio of 1, indicating no difference between the two samples, is depicted by the dashed line on each graph, and asterisks indicates statistically significant deviations from a value of 1 ($P \leq 0.05$). With the exception of CMP, Rif treatment decreased the abundances of NMPs. In contrast, the abundances of all four NTPs increased. These results suggested that Rif treatment led to the inhibition of the RNA futile cycle, which consequently increased the energy level of cells.

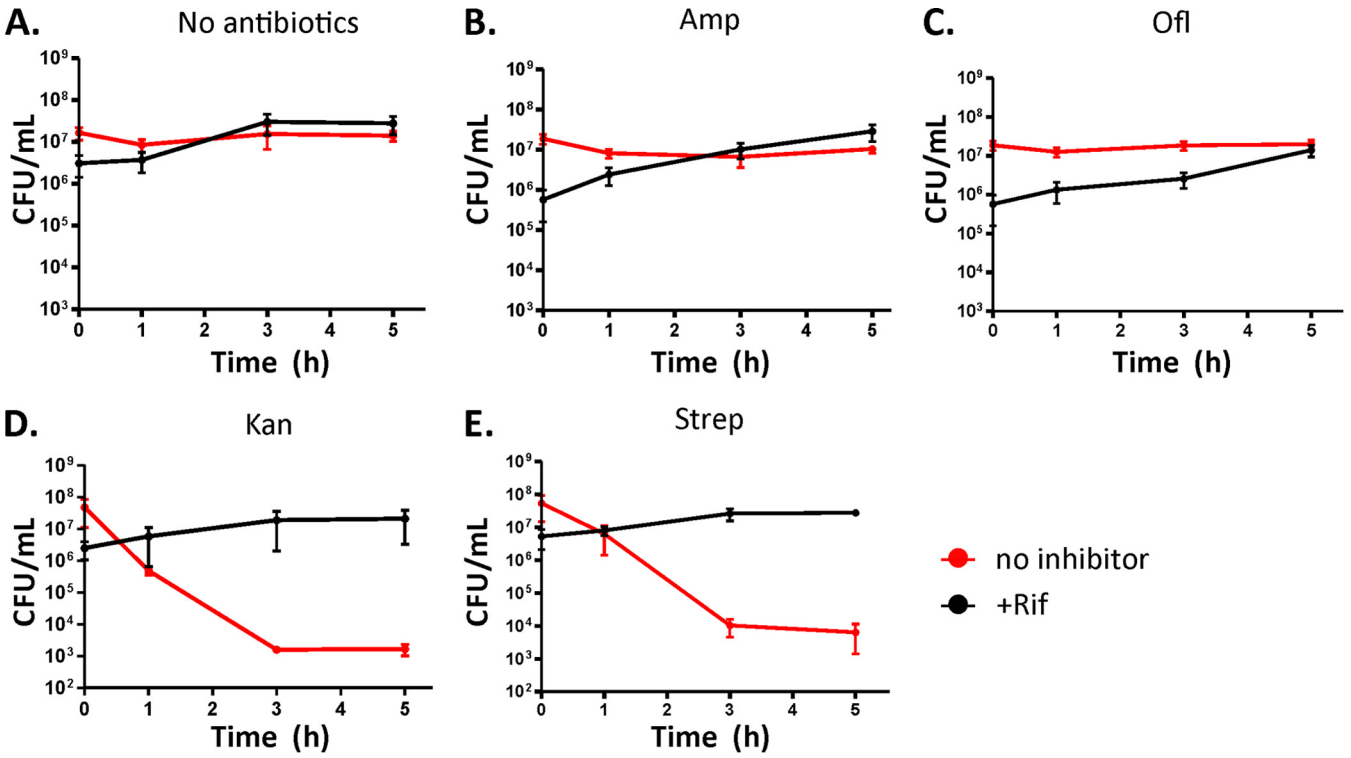

FIG 7 Effect of inhibiting the RNA futile cycle on the antibiotic tolerances of MazF persisters. *E. coli* MO::*mazE-mazF* was diluted in Gutnick-glucose medium supplemented with aTc, cultured for 3 h, and treated with no inhibitor or Rif. One hour posttreatment, cells were exposed to no antibiotics (A), Amp (B), Ofl (C), Kan (D), or Strep (E). Rif treatment caused reduced culturability at time zero, which was regained during the course of the assay (refer to Fig. S6 in the supplemental material for supporting data). In MazF-accumulating cells, Rif treatment did not alter Amp or Ofl persister levels compared with the untreated control. However, MazF-accumulating cells were sensitive to Kan and Strep, and an increase in persister levels was observed only when transcription and, as a consequence, translation were inhibited with Rif treatment.

with other toxins, will help define the phenotypic landscape of persisters and shed light on their vulnerabilities.

MATERIALS AND METHODS

Bacterial strains and plasmids. *E. coli* MO::*mazE* and *E. coli* MO::*mazE-mazF* are derivatives of *E. coli* MO001 (53), which harbors an inducible copy of the mCherry gene in place of *lacZYA*. Additional description and methods for their construction are provided in Text S1 in the supplemental material. Bacterial strains, plasmids, and primers for plasmid and strain construction that were used in this study are presented in Table S1 in the supplemental material.

Chemicals and growth medium. Growth medium components, inducers, and antibiotics were purchased from Thermo, Fisher Scientific (Waltham, MA) or Sigma-Aldrich (St. Louis, MO). Methods for their preparation are detailed in the Text S1 in the supplemental material. Overall, we used 100 mM Ara to induce *mazE* and 300 ng/ml aTc to induce *mazF* to ensure high MazF accumulation throughout the course of the experiments. We also demonstrated that reducing the inducer concentration to 50 or 150 ng/ml produced comparable growth inhibition and persister phenotypes (see Fig. S8A to C in the supplemental material).

Culture conditions and growth measurements. Unless otherwise described, overnight cultures were inoculated from to −80°C stocks stored in 15% glycerol and grown in 2 ml of Luria-Bertani (LB) medium in a test tube with shaking at 250 rpm for 4 h before being diluted (1:100) in 2 ml of Gutnick medium (66) with 10 mM glucose in a test tube and grown for an additional 16 h. Following overnight growth, cells were diluted in 25 ml of Gutnick-glucose supplemented with 100 mM Ara (to induce *mazE* in both MO::*mazE* and MO::*mazE-mazF*) to an OD_{600} of ~0.01 and grown at 37°C with shaking at 250 rpm. After approximately one doubling, cells were induced with 300 ng/ml aTc (to induce *mazF* in MO::*mazE-mazF*). When the OD_{600} of these initial cultures had reached 0.1, 5 ml of cells was pelleted by centrifugation at 4,000 rpm at 37°C for 10 min. After removal of 4 ml of supernatant, the pellet was resuspended in the remaining medium and transferred to a microcentrifuge tube, where it was pelleted at 15,000 rpm for 3 min. After removal of the remaining supernatant, the pellets were washed with prewarmed (37°C) Gutnick-glucose medium and centrifuged again. The pellets were then resuspended and reinoculated into 25 ml of prewarmed Gutnick-glucose medium supplemented with either aTc or aTc and Ara to achieve an OD_{600} of 0.02. At designated time points, samples were collected for OD_{600} measurements (measured using the BioTek Synergy H1 multimode reader; Biotek Instruments, Inc., Winooski, VT) and CFU enumeration. To enumerate CFU per milliliter, 500 μl of samples was collected, and the cells were pelleted by centrifugation at 15,000 rpm for 3 min. After removal of 450 μl of supernatant, the pellets were washed with 450 μl of 1× phosphate-buffered saline (PBS). Cells were pelleted again by centrifugation, and 400 μl of supernatant was removed. The pellets were resuspended in the remaining 100 μl of PBS and transferred to individual wells of a 96-well round-bottom plate. Ten microliters of each sample was serially diluted in 90 μl of PBS, and 10 μl of each dilution was spotted onto LB agar plates supplemented with Ara. The plates were incubated at 37°C for 16 h before CFU were counted. For each data point, 10 to 100 colonies were counted. Where indicated, 450 μl of washed cells was mixed with 50 μl Sphero AccuCount fluorescent particles (Spherotech Inc., Lake Forest, IL), and cells were enumerated using an LSRII flow cytometer (BD Biosciences, San Jose, CA). Cell populations and fluorescent particles were detected and distinguished using forward and side scattering parameters, and the particles were further identified by measuring green fluorescence

(488-nm laser, 525/50-nm band pass filter). Data were acquired and analyzed using the FACSDiva software.

Persister assay. Overnight cultures were inoculated, cultured, induced, washed, and diluted as described above. At specified time points or cell densities following dilution in Gutnick-glucose with aTc or aTc and Ara, 500-μl aliquots of culture were transferred into 17- by 100-mm polypropylene test tubes (Thermo, Fisher Scientific), treated with antibiotics, and incubated at 37°C with shaking at 250 rpm. At designated time points, cells were transferred into microcentrifuge tubes, pelleted by centrifugation at 15,000 rpm for 3 min, and washed twice with PBS to reduce antibiotic concentrations to below their MICs (67). Samples were serially diluted in PBS, and 10 μl of each dilution was plated on LB-agar with Ara. When necessary, the entire 90-μl sample was plated in order to improve the limit of detection. The plates were then incubated at 37°C for 16 h. For each data point, 10 to 100 colonies were counted following incubation.

Oxygen and glucose consumption assays. When the OD_{600} of the initial cultures reached 0.1, 2 ml of culture was transferred to microcentrifuge tubes, pelleted by centrifugation (15,000 rpm, 3 min), and washed with 2 ml of warmed medium (Gutnick with 2 mM glucose supplemented with aTc or aTc and Ara). Oxygen measurements were carried out in a disposable bioreactor following previously published protocols (47, 68). Briefly, cells were inoculated in 10 ml of warm medium in a 50-ml Falcon tube in which the medium is stirred with a sterilized magnetic stirring bar. The Falcon tube was further immersed in a stirred water bath to maintain the temperature at 37°C. The concentration of dissolved oxygen was measured for 5 h using the FireSting O2 fiber-optic O_2 meter with an OXF1100 fixed-needle-type minisensor (PyroScience GmbH). The temperature of the water bath was monitored using the TDIP15 temperature sensor (PyroScience GmbH) so that signals from the O_2 sensor could be automatically adjusted for temperature fluctuations. We note that the equilibrium concentration of O_2 in the medium in contact with air is ~210 μM (47). Three hours postinoculation, inhibitors, such as Rif, Spec, and KCN, were added. Every 30 min throughout the course of the experiment, 200 μl of culture was taken for OD_{600} measurements, and the sample was filtered using a 0.22-μm filter. The filtrates were collected and stored at −20°C until they were used for glucose measurements, which were made using an Amplex Red glucose/glucose oxidase kit (Life Technologies). Total O_2 consumed was calculated using the approach reported by Adolfsen and Brynildsen (47). The volumetric mass transfer coefficient (k_La) used for this calculation was determined by purging cell-free Gutnick-glucose medium with N_2 and calculating the slope of the continuous increase in dissolved O_2 versus time. k_La was measured for 8, 9, and 10 ml of medium in order to obtain a regression equation [$k_La(V) = -0.7993V + 12.707$, where V is the volume of culture in the bioreactor and this linear fit yielded an R^2 value of 1] to determine the k_La that was to be used for each data point as the volume of the culture decreased throughout the course of the assay due to sampling. Total glucose consumed was calculated by subtracting glucose concentration measured in the filtrate collected at each time point from 2 mM (concentration at time zero). To calculate amounts of oxygen and glucose consumed per biomass, total oxygen or glucose consumed between 2.5 and 5 h of the assay (once MazF-mediated growth inhibition was achieved) was plotted against OD_{600} measured during that time, and linear regression was performed to obtain the slopes of the regression lines.

LC-MS metabolomic analysis. To extract cellular metabolites, metabolism was quickly quenched by vacuum-filtering 4 ml of culture at designated time points on nylon membranes (0.45-μm pore size) and transferring these membranes into 60-mm petri dishes containing 1.2 ml of cold (−20°C) extraction solvent (40:40:20 methanol/acetonitrile/H_2O, high-performance liquid chromatography [HPLC] grade). Culture density at the time of extraction was measured by OD_{600}. After 30 min of extraction at −20°C, membranes were thoroughly washed with extraction solvent in the dish. The extracts were collected in microcentrifuge tubes and centrifuged at 15,000 rpm at 4°C for 5 min, and 300 μl of supernatant from each sample was transferred to new microcentrifuge tubes. To obtain soluble metabolites, the supernatants were dried under N_2 gas and resuspended in HPLC-grade H_2O. Samples were analyzed by reversed-phase ion-pairing liquid chromatography coupled to a stand-alone Orbitrap mass spectrometer (Exactive; Thermo Scientific) by negative-ion mode electrospray ionization (69). Metabolite peaks that matched both exact mass-to-charge ratios and retention times of authenticated standards were quantified using MAVEN software (70). Metabolite abundances were normalized to cell density (OD_{600}). Ratios of normalized ribonucleotide abundances in samples cultured in the presence of aTc to abundances in samples cultured in the presence of aTc and Ara were calculated to determine the effect of MazF accumulation. For samples treated with inhibitors, ratios of normalized ribonucleotide abundances of treated samples to untreated samples were calculated to assess the impact of inhibitor treatment.

Statistical analysis. At least three biological replicates were performed for each experimental condition. Where indicated, a two-tailed t test was performed for pairwise comparisons. P values of ≤ 0.05 were considered significant, and each data point was represented by the mean value and the standard error.

SUPPLEMENTAL MATERIAL

Supplemental material for this article may be found at http://mbio.asm.org/lookup/suppl/doi:10.1128/mBio.01588-15/-/DCSupplemental.

Text S1, DOCX file, 0.03 MB.
Figure S1, TIF file, 0.3 MB.
Figure S2, TIF file, 0.1 MB.
Figure S3, TIF file, 2.5 MB.
Figure S4, TIF file, 0.4 MB.
Figure S5, TIF file, 0.3 MB.
Figure S6, TIF file, 0.2 MB.
Figure S7, TIF file, 0.2 MB.
Figure S8, TIF file, 0.2 MB.
Table S1, DOCX file, 0.02 MB.

ACKNOWLEDGMENTS

We are grateful to Kristin Adolfsen, Jonathan Robinson, Theresa Henry, Mehmet Orman, Katherine Völzing, Ludwik Gorczyca, and Stephanie Amato for technical assistance. We thank Christina De Coste and the Molecular Biology Flow Cytometry Resource Facility which is partially supported by the Cancer Institute of New Jersey Cancer Center Support Grant (P30CA072720).

Financial support was provided by the Army Research Office (W911NF-15-1-0173) and the National Institute of Allergy and Infectious Diseases of the National Institutes of Health (R21AI105342).

The content is solely the responsibility of the authors and does not necessarily represent the official views of the Army Research Office, National Institutes of Health, or Princeton University. The funders had no role in study design, data collection and analysis, decision to publish, or preparation of the manuscript.

We declare that no competing interests exist.

REFERENCES

1. **Lewis K**. 2010. Persister cells. Annu Rev Microbiol **64**:357–372. http://dx.doi.org/10.1146/annurev.micro.112408.134306.
2. **Bigger J**. 1944. Treatment of staphylococcal infections with penicillin by intermittent sterilisation. Lancet **244**:497–500. http://dx.doi.org/10.1016/S0140-6736(00)74210-3.
3. **Maisonneuve E, Gerdes K**. 2014. Molecular mechanisms underlying bacterial persisters. Cell **157**:539–548. http://dx.doi.org/10.1016/j.cell.2014.02.050.
4. **Fauvart M, De Groote VN, Michiels J**. 2011. Role of persister cells in chronic infections: clinical relevance and perspectives on anti-persister therapies. J Med Microbiol **60**:699–709. http://dx.doi.org/10.1099/jmm.0.030932-0.
5. **Grant SS, Hung DT**. 2013. Persistent bacterial infections, antibiotic tolerance, and the oxidative stress response. Virulence **4**:273–283. http://dx.doi.org/10.4161/viru.23987.

6. **Cohen N, Lobritz M, Collins J.** 2013. Microbial persistence and the road to drug resistance. Cell Host Microbe **13:**632–642. http://dx.doi.org/10.1016/j.chom.2013.05.009.
7. **Gefen O, Balaban NQ.** 2009. The importance of being persistent: heterogeneity of bacterial populations under antibiotic stress. FEMS Microbiol Rev **33:**704–717. http://dx.doi.org/10.1111/j.1574-6976.2008.00156.x.
8. **Wakamoto Y, Dhar N, Chait R, Schneider K, Signorino-Gelo F, Leibler S, McKinney JD.** 2013. Dynamic persistence of antibiotic-stressed mycobacteria. Science **339:**91–95. http://dx.doi.org/10.1126/science.1229858.
9. **Orman MA, Brynildsen MP.** 2013. Establishment of a method to rapidly assay bacterial persister metabolism. Antimicrob Agents Chemother **57:**4398–4409. http://dx.doi.org/10.1128/AAC.00372-13.
10. **Allison KR, Brynildsen MP, Collins JJ.** 2011. Metabolite-enabled eradication of bacterial persisters by aminoglycosides. Nature **473:**216–220. http://dx.doi.org/10.1038/nature10069.
11. **Barraud N, Buson A, Jarolimek W, Rice SA.** 2013. Mannitol enhances antibiotic sensitivity of persister bacteria in Pseudomonas aeruginosa biofilms. PLoS One **8:**e84220. http://dx.doi.org/10.1371/journal.pone.0084220.
12. **Mok WWK, Orman MA, Brynildsen MP.** 2015. Impacts of global transcriptional regulators on persister metabolism. Antimicrob Agents Chemother **59:**2713–2719. http://dx.doi.org/10.1128/AAC.04908-14.
13. **Prax M, Bertram R.** 2014. Metabolic aspects of bacterial persisters. Front Cell Infect Microbiol **4:**148. http://dx.doi.org/10.3389/fcimb.2014.00148.
14. **Amato SM, Fazen CH, Henry TC, Mok WWK, Orman MA, Sandvik EL, Volzing KG, Brynildsen MP.** 2014. The role of metabolism in bacterial persistence. Front Microbiol **5:**70. http://dx.doi.org/10.3389/fmicb.2014.00070.
15. **Shan Y, Lazinski D, Rowe S, Camilli A, Lewis K.** 2015. Genetic basis of persister tolerance to aminoglycosides in *Escherichia coli*. mBio **6:**e00078-15. http://dx.doi.org/10.1128/mBio.00078-15.
16. **Spoering AL, Vulic M, Lewis K.** 2006. GlpD and PlsB participate in persister cell formation in *Escherichia coli*. J Bacteriol **188:**5136–5144. http://dx.doi.org/10.1128/JB.00369-06.
17. **Girgis HS, Harris K, Tavazoie S.** 2012. Large mutational target size for rapid emergence of bacterial persistence. Proc Natl Acad Sci U S A **109:**12740–12745. http://dx.doi.org/10.1073/pnas.1205124109.
18. **Ma C, Sim S, Shi W, Du L, Xing D, Zhang Y.** 2010. Energy production genes sucB and ubiF are involved in persister survival and tolerance to multiple antibiotics and stresses in *Escherichia coli*. FEMS Microbiol Lett **303:**33–40.
19. **Amato S, Orman M, Brynildsen M.** 2013. Metabolic control of persister formation in *Escherichia coli*. Mol Cell **50:**475–487. http://dx.doi.org/10.1016/j.molcel.2013.04.002.
20. **Amato SM, Brynildsen MP.** 2014. Nutrient transitions are a source of persisters in *Escherichia coli* biofilms. PLoS One **9:**e93110. http://dx.doi.org/10.1371/journal.pone.0093110.
21. **Bernier SP, Lebeaux D, DeFrancesco AS, Valomon A, Soubigou G, Coppée J, Ghigo J, Beloin C.** 2013. Starvation, together with the SOS response, mediates high biofilm-specific tolerance to the fluoroquinolone ofloxacin. PLoS Genet **9:**e1003144. http://dx.doi.org/10.1371/journal.pgen.1003144.
22. **Lebeaux D, Chauhan A, Létoffé S, Fischer F, de Reuse H, Beloin C, Ghigo J-.** 2014. pH-mediated potentiation of aminoglycosides kills bacterial persisters and eradicates in vivo biofilms. J Infect Dis **210:**1357–1366. http://dx.doi.org/10.1093/infdis/jiu286.
23. **Kim J-S, Heo P, Yang T-J, Lee K-S, Cho D-H, Kim BT, Suh J-H, Lim H-J, Shin D, Kim S-K, Kweon D-H.** 2011. Selective killing of bacterial persisters by a single chemical compound without affecting normal antibiotic-sensitive cells. Antimicrob Agents Chemother **55:**5380–5383. http://dx.doi.org/10.1128/AAC.00708-11.
24. **Luidalepp H, Jõers A, Kaldalu N, Tenson T.** 2011. Age of inoculum strongly influences persister frequency and can mask effects of mutations implicated in altered persistence. J Bacteriol **193:**3598–3605. http://dx.doi.org/10.1128/JB.00085-11.
25. **Roostalu J, Jõers A, Luidalepp H, Kaldalu N, Tenson T.** 2008. Cell division in *Escherichia coli* cultures monitored at single cell resolution. BMC Microbiol **8:**68. http://dx.doi.org/10.1186/1471-2180-8-68.
26. **Ayrapetyan M, Williams TC, Baxter R, Oliver JD.** 2015. Viable but nonculturable and persister cells coexist stochastically and are induced by human serum. Infect Immun **83:**4194–4203. http://dx.doi.org/10.1128/IAI.00404-15.
27. **Keren I, Shah D, Spoering A, Kaldalu N, Lewis K.** 2004. Specialized persister cells and the mechanism of multidrug tolerance in *Escherichia coli*. J Bacteriol **186:**8172–8180. http://dx.doi.org/10.1128/JB.186.24.8172-8180.2004.
28. **Cañas-Duarte SJ, Restrepo S, Pedraza JM.** 2014. Novel protocol for persister cells isolation. PLoS One **9:**e88660.
29. **Shah D, Zhang Z, Khodursky A, Kaldalu N, Kurg K, Lewis K.** 2006. Persisters: a distinct physiological state of *E. coli*. BMC Microbiol **6:**53. http://dx.doi.org/10.1186/1471-2180-6-53.
30. **Bokinsky G, Baidoo EEK, Akella S, Burd H, Weaver D, Alonso-Gutierrez J, García-Martín H, Lee TS, Keasling JD.** 2013. HipA-triggered growth arrest and β-lactam tolerance in *Escherichia coli* are mediated by RelA-dependent ppGpp synthesis. J Bacteriol **195:**3173–3182. http://dx.doi.org/10.1128/JB.02210-12.
31. **Vázquez-Laslop N, Lee H, Neyfakh AA.** 2006. Increased persistence in *Escherichia coli* caused by controlled expression of toxins or other unrelated proteins. J Bacteriol **188:**3494–3497. http://dx.doi.org/10.1128/JB.188.10.3494-3497.2006.
32. **Verstraeten N, Knapen W, Kint C, Liebens V, Van den Bergh B, Dewachter L, Michiels J, Fu Q, David C, Fierro A, Marchal K, Beirlant J, Versées W, Hofkens J, Jansen M, Fauvart M, Michiels J.** 2015. Obg and membrane depolarization are part of a microbial bet-hedging strategy that leads to antibiotic tolerance. Mol Cell **59:**9–21. http://dx.doi.org/10.1016/j.molcel.2015.05.011.
33. **Kwan BW, Valenta JA, Benedik MJ, Wood TK.** 2013. Arrested protein synthesis increases persister-like cell formation. Antimicrob Agents Chemother **57:**1468–1473. http://dx.doi.org/10.1128/AAC.02135-12.
34. **Gerdes K, Maisonneuve E.** 2012. Bacterial persistence and toxin-antitoxin loci. Annu Rev Microbiol **66:**103–123. http://dx.doi.org/10.1146/annurev-micro-092611-150159.
35. **Yamaguchi Y, Park J, Inouye M.** 2011. Toxin-antitoxin systems in bacteria and archaea. Annu Rev Genet **45:**61–79. http://dx.doi.org/10.1146/annurev-genet-110410-132412.
36. **Goeders N, Van Melderen L.** 2014. Toxin-antitoxin systems as multilevel interaction systems. Toxins (Basel) **6:**304–324. http://dx.doi.org/10.3390/toxins6010304.
37. **Van Melderen L.** 2010. Toxin-antitoxin systems: why so many, what for? Curr Opin Microbiol **13:**781–785. http://dx.doi.org/10.1016/j.mib.2010.10.006.
38. **Germain E, Roghanian M, Gerdes K, Maisonneuve E.** 2015. Stochastic induction of persister cells by HipA through (p)ppGpp-mediated activation of mRNA endonucleases. Proc Natl Acad Sci U S A **112:**5171–5176. http://dx.doi.org/10.1073/pnas.1423536112.
39. **Aizenman E, Engelberg-Kulka H, Glaser G.** 1996. An *Escherichia coli* chromosomal "addiction module" regulated by guanosine [corrected] 3′,5′-bispyrophosphate: a model for programmed bacterial cell death. Proc Natl Acad Sci U S A **93:**6059–6063. http://dx.doi.org/10.1073/pnas.93.12.6059.
40. **Zhang Y, Zhang J, Hoeflich KP, Ikura M, Qing G, Inouye M.** 2003. MazF cleaves cellular mRNAs specifically at ACA to block protein synthesis in *Escherichia coli*. Mol Cell **12:**913–923. http://dx.doi.org/10.1016/S1097-2765(03)00402-7.
41. **Amitai S, Kolodkin-Gal I, Hananya-Meltabashi M, Sacher A, Engelberg-Kulka H.** 2009. *Escherichia coli* MazF leads to the simultaneous selective synthesis of both "death proteins" and "survival proteins". PLoS Genet **5:**e1000390. http://dx.doi.org/10.1371/journal.pgen.1000390.
42. **Amitai S, Yassin Y, Engelberg-Kulka H.** 2004. MazF-mediated cell death in *Escherichia coli*: a point of no return. J Bacteriol **186:**8295–8300. http://dx.doi.org/10.1128/JB.186.24.8295-8300.2004.
43. **Pedersen K, Christensen SK, Gerdes K.** 2002. Rapid induction and reversal of a bacteriostatic condition by controlled expression of toxins and antitoxins. Mol Microbiol **45:**501–510. http://dx.doi.org/10.1046/j.1365-2958.2002.03027.x.
44. **Tripathi A, Dewan PC, Siddique SA, Varadarajan R.** 2014. MazF-induced growth inhibition and persister generation in *Escherichia coli*. J Biol Chem **289:**4191–4205. http://dx.doi.org/10.1074/jbc.M113.510511.
45. **Lutz R, Bujard H.** 1997. Independent and tight regulation of transcriptional units in *Escherichia coli* via the LacR/O, the TetR/O and AraC/I1-I2 regulatory elements. Nucleic Acids Res **25:**1203–1210. http://dx.doi.org/10.1093/nar/25.6.1203.
46. **Robinson JL, Miller RV, Brynildsen MP.** 2014. Model-driven identification of dosing regimens that maximize the antimicrobial activity of nitric oxide. Metab Eng Commun **1:**12–18.
47. **Adolfsen KJ, Brynildsen MP.** 2015. Futile cycling increases sensitivity

toward oxidative stress in *Escherichia coli*. Metab Eng **29:**26–35. http://dx.doi.org/10.1016/j.ymben.2015.02.006.
48. **Izallalen M, Mahadevan R, Burgard A, Postier B, Didonato R, Sun J, Schilling CH, Lovley DR**. 2008. Geobacter sulfurreducens strain engineered for increased rates of respiration. Metab Eng **10:**267–275. http://dx.doi.org/10.1016/j.ymben.2008.06.005.
49. **Bennett BD, Yuan J, Kimball EH, Rabinowitz JD**. 2008. Absolute quantitation of intracellular metabolite concentrations by an isotope ratio-based approach. Nat Protoc **3:**1299–1311. http://dx.doi.org/10.1038/nprot.2008.107.
50. **Bennett BD, Kimball EH, Gao M, Osterhout R, Van Dien SJ, Rabinowitz JD**. 2009. Absolute metabolite concentrations and implied enzyme active site occupancy in *Escherichia coli*. Nat Chem Biol **5:**593–599. http://dx.doi.org/10.1038/nchembio.186.
51. **Chapman AG, Fall L, Atkinson DE**. 1971. Adenylate energy charge in *Escherichia coli* during growth and starvation. J Bacteriol **108:**1072–1086.
52. **Vesper O, Amitai S, Belitsky M, Byrgazov K, Kaberdina A, Engelberg-Kulka H, Moll I**. 2011. Selective translation of leaderless mRNAs by specialized ribosomes generated by MazF in *Escherichia coli*. Cell **147:**147–157. http://dx.doi.org/10.1016/j.cell.2011.07.047.
53. **Orman MA, Brynildsen MP**. 2013. Dormancy is not necessary or sufficient for bacterial persistence. Antimicrob Agents Chemother **57:**3230–3239. http://dx.doi.org/10.1128/AAC.00243-13.
54. **Suzuki M, Zhang J, Liu M, Woychik NA, Inouye M**. 2005. Single protein production in living cells facilitated by an mRNA interferase. Mol Cell **18:**253–261. http://dx.doi.org/10.1016/j.molcel.2005.03.011.
55. **Davies J, Davis BD**. 1968. Misreading of ribonucleic acid code words induced by aminoglycoside antibiotics. The effect of drug concentration. J Biol Chem **243:**3312–3316.
56. **Moazed D, Noller HF**. 1987. Interaction of antibiotics with functional sites in 16S ribosomal RNA. Nature **327:**389–394. http://dx.doi.org/10.1038/327389a0.
57. **Gromadski KB, Rodnina MV**. 2004. Streptomycin interferes with conformational coupling between codon recognition and GTPase activation on the ribosome. Nat Struct Mol Biol **11:**316–322. http://dx.doi.org/10.1038/nsmb742.
58. **Shapiro HM**. 2000. Membrane potential estimation by flow cytometry. Methods **21:**271–279. http://dx.doi.org/10.1006/meth.2000.1007.
59. **Taber HW, Mueller JP, Miller PF, Arrow AS**. 1987. Bacterial uptake of aminoglycoside antibiotics. Microbiol Res **51:**439–457.
60. **Ramos S, Schuldiner S, Kaback HR**. 1976. The electrochemical gradient of protons and its relationship to active transport in *Escherichia coli* membrane vesicles. Proc Natl Acad Sci U S A **73:**1892–1896. http://dx.doi.org/10.1073/pnas.73.6.1892.
61. **Erental A, Sharon I, Engelberg-Kulka H**. 2012. Two programmed cell death systems in *Escherichia coli*: an apoptotic-like death is inhibited by the mazEF-mediated death pathway. PLoS Biol **10:**e1001281. http://dx.doi.org/10.1371/journal.pbio.1001281.
62. **Rotem E, Loinger A, Ronin I, Levin-Reisman I, Gabay C, Shoresh N, Biham O, Balaban NQ**. 2010. Regulation of phenotypic variability by a threshold-based mechanism underlies bacterial persistence. Proc Natl Acad Sci U S A **107:**12541–12546. http://dx.doi.org/10.1073/pnas.1004333107.
63. **Allison KR, Brynildsen MP, Collins JJ**. 2011. Heterogeneous bacterial persisters and engineering approaches to eliminate them. Curr Opin Microbiol **14:**593–598. http://dx.doi.org/10.1016/j.mib.2011.09.002.
64. **Orman MA, Brynildsen MP**. 2015. Inhibition of stationary phase respiration impairs persister formation in *E. coli*. Nat Commun **6:**7983.
65. **Kasari V, Mets T, Tenson T, Kaldalu N**. 2013. Transcriptional cross-activation between toxin-antitoxin systems of *Escherichia coli*. BMC Microbiol **13:**45. http://dx.doi.org/10.1186/1471-2180-13-45.
66. **Gutnick D, Calvo JM, Klopotowski T, Ames BN**. 1969. Compounds which serve as the sole source of carbon or nitrogen for Salmonella typhimurium LT-2. J Bacteriol **100:**215–219.
67. **Andrews JM**. 2001. Determination of minimum inhibitory concentrations. J Antimicrob Chemother **48**(Suppl 1):5–16. http://dx.doi.org/10.1093/jac/48.suppl_1.5.
68. **Robinson JL, Brynildsen MP**. 2013. A kinetic platform to determine the fate of nitric oxide in *Escherichia coli*. PLoS Comput Biol **9:**e1003049. http://dx.doi.org/10.1371/journal.pcbi.1003049.
69. **Lu W, Clasquin MF, Melamud E, Amador-Noguez D, Caudy AA, Rabinowitz JD**. 2010. Metabolomic analysis via reversed-phase ion-pairing liquid chromatography coupled to a stand alone Orbitrap mass spectrometer. Anal Chem **82:**3212–3221. http://dx.doi.org/10.1021/ac902837x.
70. **Melamud E, Vastag L, Rabinowitz JD**. 2010. Metabolomic analysis and visualization engine for LC-MS data. Anal Chem **82:**9818–9826. http://dx.doi.org/10.1021/ac1021166.
71. **Guzman LM, Belin D, Carson MJ, Beckwith J**. 1995. Tight regulation, modulation, and high-level expression by vectors containing the arabinose PBAD promoter. J Bacteriol **177:**4121–4130.
72. **Datsenko KA, Wanner BL**. 2000. One-step inactivation of chromosomal genes in *Escherichia coli* K-12 using PCR products. Proc Natl Acad Sci U S A **97:**6640–6645. http://dx.doi.org/10.1073/pnas.120163297.
73. **Zaslaver A, Bren A, Ronen M, Itzkovitz S, Kikoin I, Shavit S, Liebermeister W, Surette MG, Alon U**. 2006. A comprehensive library of fluorescent transcriptional reporters for *Escherichia coli*. Nat Methods **3:**623–628.